Sub Topic: Turbulent Flames

SAND2019-11722C

2019 WSSCI Fall Technical Meeting
Organized by the Western States Section of the Combustion Institute
October 14–15, 2019
Albuquerque, New Mexico

Soot and radiation interactions in turbulent jet flames studied with Reynolds-averaged Navier-Stokes simulations

Alexandra Baumgart[1], *Tyler Voskuilen*[2], *Philip Sakievich*[2], *and John Hewson*[1,*]

[1]*Fire Science and Technology, Sandia National Laboratories, PO Box 5800, MS 1135, Albuquerque, NM 87185-1135, USA*
[2]*Computational Thermodynamics and Fluid Mechanics, Sandia National Laboratories, PO Box 5800, MS 0828, Albuquerque, NM 87185-0828, USA*
[*]*Corresponding author:* jchewso@sandia.gov

Abstract: Soot and radiation heat losses are both affected by finite residence times in turbulent hydrocarbon flames. This computational study aims to understand the effects of flow conditions and model parameters on the soot and enthalpy evolution in turbulent jet flames. Jet flames burning in air are characterized by a residence time, or the fuel-air mixing time. This time scale limits the time available for other processes to occur, including soot formation and radiation heat transfer. The inlet jet velocity, sooting tendency of the fuel, and fuel density were varied in Reynolds-averaged Navier-Stokes (RANS) simulations with standard k-ε closure models. Presumed-PDF flamelet libraries for ethene and heptane model the main flame chemistry and provide soot and radiation source terms. The tendency of the fuel to form soot was varied artificially through a factor applied to the soot source terms. The parameters studied were found to have competing effects on the residence time, soot formation, and radiation losses of the jet flame. Longer residence times led to increased soot formation and radiation, until the increase in radiation began to limit further soot formation.
Keywords: ***soot, radiation, turbulent flames***

1. Introduction

Thermal radiation is an important contributor to heat transfer in fires and practical combustors, and for hydrocarbon fuels soot is a significant contributor to this radiation heat transfer. However, soot evolution and radiation heat transfer are among the slower processes and are often affected by the fuel-air mixing rates. The manner in which global mixing rates affect local and global soot levels has been addressed recently over a certain range of parameter space [1]. This supplements earlier understanding that global radiation heat transfer from jet flames tends to increase as the global residence time increases [2]. More recent work has shown possibly non-monotonic behavior in the global radiant emissions as a function of the residence time, or at least as a function of d/u, where d is the jet nozzle diameter and u is the jet exit velocity [3]. Understanding of the relative significance of time scales for fuel-air mixing, soot evolution, and radiation heat transfer is important for predicting trends in heat transfer in fires and combustors. Modeling studies offer potential insights into the relationship between the physics and the resulting behavior because the model can be queried more fully than experiments.

This work uses relatively simple computational models to predict soot and enthalpy evolution in turbulent jet flames, providing a framework for discussing time scale interactions and assessing the ability of this class of models to predict in more highly sooting environments through scaling arguments. The core combustion modeling approach is based on flamelet methods [4, 5] where the thermochemical state

is referenced to a reduced set of variables that evolves in the computational fluid dynamics (CFD) used to predict the overall flow field evolution. The temperature, species mass fractions, and needed source terms are primarily related to evolved variables such as mixture fraction and enthalpy and derived variables such as scalar dissipation rate. These dependent variables can then be expressed using a flamelet library where the independent variables are taken from the CFD-level solution.

Flamelet methods have been applied to similar problems addressing soot formation and radiation losses in turbulent jet flames. Early work, including [6–8], pioneered the approaches employed here to bring soot and enthalpy evolution into the flamelet methodology. These methods developed empirical two-equation models for soot evolution, based on a soot number density and mass density (equivalently, mass fraction or volume fraction) that used the local temperature and species information (often C_2H_2) from the flamelet library to provide source and sink terms for soot. Similarly, radiation source terms were determined to apply to the enthalpy evolution. These two-equation soot models have been applied to a variety of fuels including methane [8], natural gas [6], ethene [7], and kerosene [9], but the source terms needed to be modified to match empirical data for each of these fuels.

More recently, a class of models has been introduced that applied the observed inverse relationship between the laminar smoke point and soot production rates [10]. This led to models that calibrated to a single fuel, generally ethene, with the source terms scaled by the laminar smoke point ratio of ethene to the target fuel [11, 12]. We note that these models generally express the soot formation as a fraction of the fuel consumption rate, which is fundamentally different from providing a kinetic two-equation model. Since the fuel consumption rate is proportional to the fuel-air mixing rate (or the scalar dissipation rate) there is a more direct dependence on the mixing rate than exists in kinetic models.

2. Methods

2.1 Conservation equations

Simulations are carried out using a low-Mach number turbulent reacting flow code (Fuego) that is a component of the Sierra suite of tools for addressing multi-physics computational science predictions [13]. The problem is formulated in the context of Reynolds-averaged Navier-Stokes (RANS) equations, including a differential buoyancy source term, with standard k-ε models to predict turbulence evolution [14]. Only conservation equations that include a source term of relevance to this analysis are given below; other standard conservation equations are not duplicated here [13].

The evolution of the enthalpy is significantly affected by radiation heat transfer in many reacting flows, and this is a focus of the present study. Enthalpy conservation is given by

$$\frac{\partial(\bar{\rho}\tilde{h})}{\partial t}+\frac{\partial(\bar{\rho}\tilde{h}\tilde{u}_j)}{\partial x_j}=\frac{\partial}{\partial x_j}\left(\left(\frac{\mu}{\mathrm{Pr}}+\frac{\mu_t}{\mathrm{Pr}_t}\right)\frac{\partial\tilde{h}}{\partial x_j}\right)-\overline{\frac{\partial q_i^r}{\partial x_i}}, \tag{1}$$

where $\tilde{h}$ is the Favre-averaged enthalpy, Pr is the Prandtl number, and Pr_t is the turbulent Prandtl number. The radiation source term in Eq.1 is the divergence of the radiant flux, $\bar{q}_i^r$, expressed as

$$\overline{\frac{\partial q_i^r}{\partial x_i}}=4\sigma\overline{\alpha T^4}-\overline{\alpha}\overline{G}, \tag{2}$$

where σ is the Stefan-Boltzmann constant, α is the absorption coefficient, and G is the radiant scalar flux. The turbulence-radiation interactions associated with the radiation emission term are treated using a presumed PDF model with a clipped Gaussian PDF parameterized using $\tilde{Z}$ and $\widetilde{Z''^2}$; this term involves contributions from both soot and gas-phase species. The absorption coefficient is expressed $\alpha=\alpha_s' Y_s+\alpha_g$, where α_s' is the soot absorption coefficient per soot mass fraction (Y_s) and α_g is the absorption coefficient of the

gas-phase components. The soot absorption coefficient expression is $\alpha_s' = (-375000 + 1735T)(\rho M)/\rho_{soot}$ [15]. The gas-phase absorption is computed in the optically thin limit using curve fits to the RADCAL database for CH_4, CO_2, H_2O, and CO [16, 17]. We note that inclusion of the single hydrocarbon, CH_4, significantly enhances the absorption coefficient for the heptane flame simulations relative to the ethene flame simulations because substantially more CH_4 is produced in heptane decomposition compared to ethene.

The fuel-air mixing is predicted through the evolution of the RANS conservation equations for the mixture fraction and its variance. The mixture fraction conservation equation

$$\frac{\partial(\bar{\rho}\tilde{Z})}{\partial t} + \frac{\partial(\bar{\rho}\tilde{Z}\tilde{u}_j)}{\partial x_j} = \frac{\partial}{\partial x_j}\left(\left(\frac{\mu}{\mathrm{Sc}} + \frac{\mu_t}{\mathrm{Sc}_t}\right)\frac{\partial \tilde{Z}}{\partial x_j}\right) + \bar{\dot{\omega}}^{Z}, \tag{3}$$

includes a source term equal in magnitude to the soot mass fraction source term ($\bar{\dot{\omega}}^{Z} = -\bar{\dot{\omega}}^{Y_s}$), with the latter given below. Soot production tends to reduce the mixture fraction, in the extreme converting a rich mixture to a stoichiometric mixture depleted of hydrocarbons suitable for soot production. Soot oxidation converts soot to CO; soot oxidation tends to increase the mixture fraction, making the mixture more rich.

Soot is modeled in the simplest manner possible through RANS conservation equations for the Favre-averaged soot number density, $\tilde{N}_s$ (in moles per mass of mixture times a gas density), and for the soot mass fraction, $\tilde{Y}_s$. Empirical source terms as a function of the temperature and acetylene concentration are obtained from literature models [8, 18, 19]. The inputs for these models are obtained from flamelet libraries.

The conservation of soot moles per mass is given by

$$\frac{\partial(\bar{\rho}\tilde{N}_s)}{\partial t} + \frac{\partial(\bar{\rho}\tilde{N}_s\tilde{u}_j)}{\partial x_j} = \frac{\partial}{\partial x_j}\left(\left(\frac{\mu}{\mathrm{Sc}} + \frac{\mu_t}{\mathrm{Sc}_t}\right)\frac{\partial \tilde{N}_s}{\partial x_j}\right) + \bar{\dot{\omega}}^{N_s}, \tag{4}$$

and the source term is

$$\bar{\dot{\omega}}^{N_s} = \overline{r_{sp} A_N [\mathrm{C_2H_2}] \exp\left(-T_N/T\right)} - \overline{\sqrt{\frac{24 v_d R T N_A}{\rho_{soot}}}\rho^2 \tilde{Y}_s^{1/6} \tilde{N}_s^{11/6}}, \tag{5}$$

where the two source terms represent nucleation and coagulation. The nucleation rate is governed by a pre-exponential coefficient $A_N = 54$ s^{-1} and an activation temperature $T_N = 21,100$ K (175 kJ mol^{-1}) and is proportional to the acetylene concentration, $[\mathrm{C_2H_2}]$. The second term represents coagulation in the free molecular limit with $v_d = [6/(\pi \rho_{soot} N_A)]^{1/3}$ used in converting the particle volume to its diameter where $\rho_{soot} = 1800$ kg/m^3 is the soot density and N_A is Avagadro's number. Particles are treated as spherical to estimate coagulation; fractal aggregates tend to have larger cross-sectional areas and agglomerate faster, reducing the particle number density, but the spherical assumption might adequately represent the primary particle surface area, providing a reasonable estimate of overall mass growth and soot volume fraction required for radiation source term estimates.

The conservation of soot mass fraction is given by

$$\frac{\partial(\bar{\rho}\tilde{Y}_s)}{\partial t} + \frac{\partial(\bar{\rho}\tilde{Y}_s\tilde{u}_j)}{\partial x_j} = \frac{\partial}{\partial x_j}\left(\left(\frac{\mu}{\mathrm{Sc}} + \frac{\mu_t}{\mathrm{Sc}_t}\right)\frac{\partial \tilde{Y}_s}{\partial x_j}\right) + \bar{\dot{\omega}}^{Y_s}. \tag{6}$$

and the source term $\bar{\dot{\omega}}^{Y_s}$ is expressed in terms of nucleation, surface growth, and OH and O_2 oxidation,

$$\begin{aligned} \bar{\dot{\omega}}^{Y_s} \;=\; & r_{sp} W_p A_N \overline{[\mathrm{C_2H_2}] \exp\left(-T_N/T\right)} \\ & + \Big[r_{sp} A_{SG} \overline{[\mathrm{C_2H_2}] \exp\left(-T_{SG}/T\right)} \\ & - A_{\mathrm{O_2}} \overline{[\mathrm{O_2}]\sqrt{T} \exp\left(-T_{\mathrm{O_2}}/T\right)} \\ & - A_{\mathrm{OH}} \overline{[\mathrm{OH}]\sqrt{T}} \Big] v_d^2 \pi \bar{\rho} \tilde{Y}_s^{2/3} \tilde{N}_s^{1/3}, \end{aligned} \tag{7}$$

where the molecular weight of a soot nucleate $W_p = 144$ kg/kmol. Surface growth and oxidation rate coefficients are $A_{SG} = 11{,}700\ \mathrm{s}^{-1}$, $T_{SG} = 12{,}000$ K, $A_{O_2} = 500\ \mathrm{s}^{-1}$, $T_{O_2} = 21{,}000$ K, and $A_{OH} = 4.23\ \mathrm{s}^{-1}$.

A factor r_{sp} adjusts the soot production rates to represent fuels with differing sooting propensities; this term applies to the nucleation and surface-growth contributions but not the oxidation. This is at best a qualitative model of varying sooting propensity, especially because aromatic fuels tend to have soot formation and growth further to the rich regions than ethene. Other groups have attempted to model PAH contributions to soot growth through other terms in the context of this two-equation soot model framework [19, 20], but in the present we do not consider this.

2.2 Simulated flames

Using the above described RANS formulation, simulations were conducted for turbulent jet flames over a wide range of parameter space. While a single jet diameter was employed in this study, the global mixing rate was varied by altering the fuel inlet velocity. Because the flame size depends on the fuel mass flow rate, model fuels of ethene and heptane were simulated with the fuel density providing an additional dimension of the parameter space. Realistic fuels are composed of mixtures of hydrocarbons, often with aromatics present. To represent the effect of fuel types including those with higher sooting propensities, the soot nucleation and surface growth rates were altered by a factor, r_{sp}, for both ethene and heptane.

The basic geometric configuration corresponds to that of Zhang et al. [21] with a 3.2 mm inner diameter fuel jet surrounded by a 15.2 mm pilot. The fuel nozzle exit velocities were set to 25, 35, 55, 70 and 100 m/s with the median velocity corresponding to measurements in [21]. A coflow of air at 0.9 m/s is also included. The range of conditions allows us to consider jointly the effects of momentum-driven mixing rates, buoyancy through flame scale, and soot production rates on the soot and enthalpy evolution. An example of predicted temperature and soot mass fraction fields is given in Fig. 1.

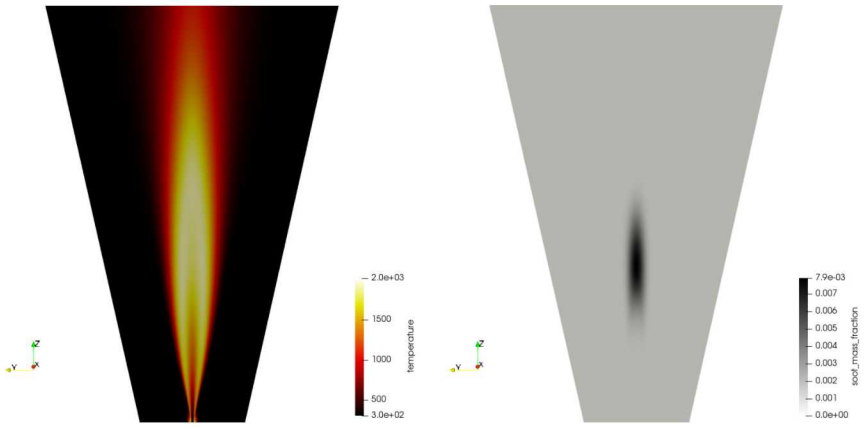

Figure 1: Contour plots of temperature and soot mass fraction for ethene jet flames with nozzle exit velocity of 54.7 m/s.

3. Results and discussion

This work focuses on the turbulent jet-flame evolution of soot and enthalpy; both evolve at rates comparable to the overall fuel-air mixing times. The relevant rates of fluid mixing are introduced next. This is followed by discussions of the effect of residence time on the soot and then the enthalpy evolution, the latter through radiant emissions. In the final subsection, modifications to the sooting propensity are simulated and the interactions of these processes discussed.

3.1 Flame evolution time scales

Fuel-air mixing is initially driven by the fuel source momentum. An initial estimate for the characteristic momentum-driven mixing time is d/u, referred to here as the convective residence time. However, buoyant acceleration can impart significant mixing energy in larger jet flames, so a more comprehensive estimate of the fuel-air mixing time is derived from the ratio of the mass of fuel in the flame to the mass flow rate of fuel from the jet. This global mixing residence time is [2]

$$\tau = \frac{\rho_f W_f^2 L_f Z_s}{3\rho_0 d^2 u}, \tag{8}$$

where ρ_f is an estimate of the flame density, W_f is the observed flame width, L_f is the observed flame length, Z_s is the stoichiometric mixture fraction, and ρ_0 is the ambient fuel density.

L_f was defined as the x-location at which the centerline carbon fraction (the sum of mixture fraction and soot mass fraction) dropped below 0.05. At $x = L_f/2$, the radial profile was used to find W_f using the same criterion. It is likely that experimental measures of flame volume used a mixture fraction threshold smaller than 0.05. To align the simulation residence times with measured residence times [2], the simulation residence times are multiplied by a factor of 5 (multiplying each length scale by a factor of about 1.7).

Simulation data for convective and global residence time is plotted together with experimental data for three hydrocarbon fuels from past work in Fig. 2 [2]. Experimental data is indicated by unfilled plot markers. As the jet velocity increases, the fuel-air mixing rate increases and both the convective residence time and global residence time decrease. Momentum-dominated jets are expected to have a slope of unity in Fig. 2. The predicted slopes of the ethene and heptane series are about 2/3 and 1/3 respectively, indicating that buoyancy affects the residence time in both flames, but the effect is stronger in heptane.

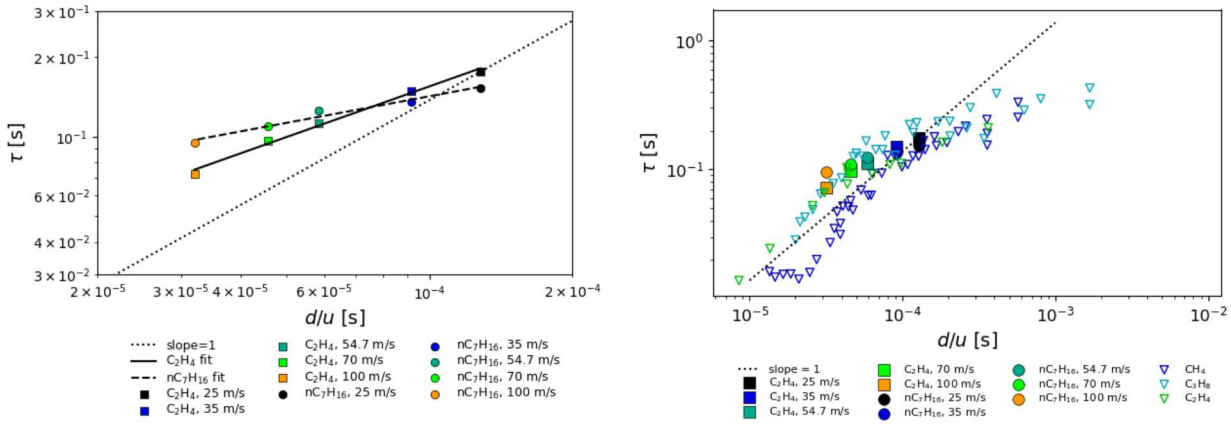

(a) Predicted τ trends.

(b) Predicted and measured τ [2].

Figure 2: The relationship between the convective residence time, d/u, and the global residence time, τ, for simulations and available literature measurements. A slope of unity is provided for reference to the momentum limit in both panels.

A more local time scale for fluid mixing is the scalar dissipation rate, describing the molecular mixing process associated with the mixture fraction. At a global level, the inverse scalar dissipation rate should scale with the global residence time, but the dissipation rates vary strongly along the flame axis as shown in Fig. 3. The scalar dissipation rate illustrates the effect of velocity on the mixing process in two respects. First, the dissipation rates scale with the source jet velocity because this provides the initial momentum-driven mixing.

Classical momentum-driven jet scaling states that $\chi \propto x^{-4}$. Second, when buoyant acceleration is more important as evident in the larger heptane jet flames, the associated buoyant acceleration slows the decay of the dissipation rate. For these larger more buoyant flames, while the dissipation rates near the flame base are smaller, the dissipation rates near the flame top are greater as evident in Fig. 3.

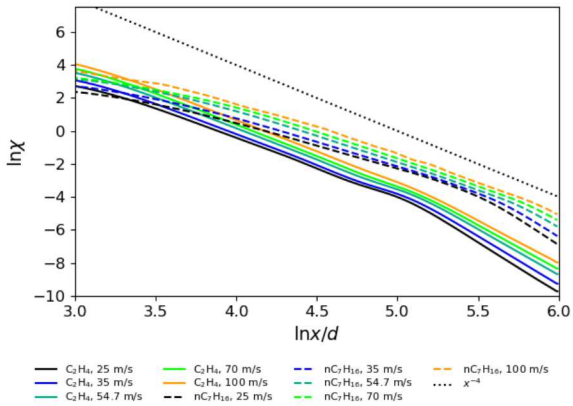

Figure 3: Predicted centerline scalar dissipation rates versus axial distance for varying jet velocity and fuel density. The larger heptane flames deviate more strongly from the x^{-4} momentum-driven limit.

3.2 Soot formation

This work begins with a basic empirical model for soot formation in ethene flames and seeks to understand the interaction between fuel-air mixing, soot evolution, and radiation enthalpy losses. We begin by assessing predictions of the well-documented Shaddix flame with the baseline ethene parameter set. Fig. 4 demonstrates reasonable agreement between predictions and measurements given the challenges of soot predictions. All predictions are conducted at a relatively low mesh resolution using the standard $k-\varepsilon$ parameter set, so jet flame heights are underpredicted. While this shifts the soot centerline profiles, other model predictions will be relative to this state.

Soot production is relatively slow in flames and is well-known to be sensitive to the global residence time. Measurements for various (relatively low-sooting) fuels show a decrease in soot levels if the global residence time is reduced, often expressed as an increase in the global strain rate [23]. Using the baseline soot model, Fig. 5a shows the centerline soot mass fractions for ethene with the jet exit velocity adjusted by factors of $\sqrt{2}$ and 2 up and down relative to the Shaddix jet flame exit velocity. Also shown are similar predictions with heptane using the same soot rate parameters (Fig. 5b); since heptane has a similar laminar smoke point to ethene, this is thought to be a reasonable first approximation subject to further validation.

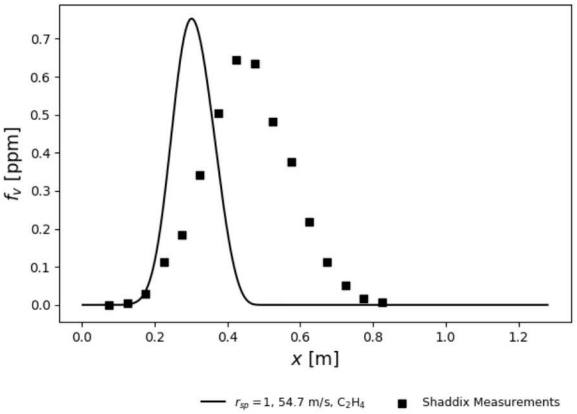

Figure 4: Centerline soot volume fraction predictions using the baseline model are compared with measurements from Shaddix [21, 22].

While the centerline soot is an often measured quantity, it is important to evaluate global soot levels. A more integral measure of the soot is the ratio of soot mass flux to fuel mass flux, referred to here as the soot fraction, χ_S. These are expressed in terms of the cross-flame area integral of the soot advection terms and mixture fraction advection terms,

$$\chi_S = \frac{Y_S''}{Z''} = \frac{\int_0^\infty \rho u Y_s r dr}{\int_0^\infty \rho u Z r dr}, \tag{9}$$

where Y_S'' and Z'' denote the integral mass fluxes of soot and mixture fraction, respectively. Profiles for the soot fraction evolution along the axis are shown in Fig. 6a where they are seen to resemble the centerline soot mass fraction in Fig. 5. In other words, the soot fraction is an integral form of the soot mass fraction that includes off-centerline contributions where significant. Since soot and radiation source terms peak off the centerline for most of the flame height, this is a better measure of the early evolution. For the ethene-based

simulations, the soot fraction decreases as jet exit velocity increases from 25-100 m/s. For the heptane-based simulations, the soot fraction increases as jet exit velocity increases from 25-54.7 m/s, then decreases from

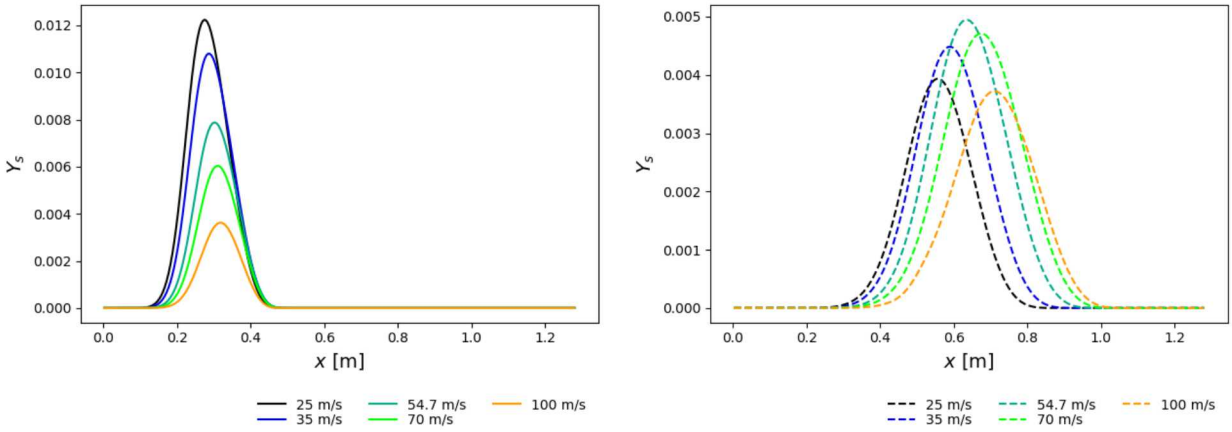

(a) Ethene axial soot mass fraction.

(b) Heptane axial soot mass fraction.

Figure 5: Effect of jet exit velocity on centerline soot mass fraction.

54.7-100 m/s. The maximum soot fractions along the flame axis for each case in Fig. 6a are extracted and plotted versus the flame residence time in Fig. 6b.

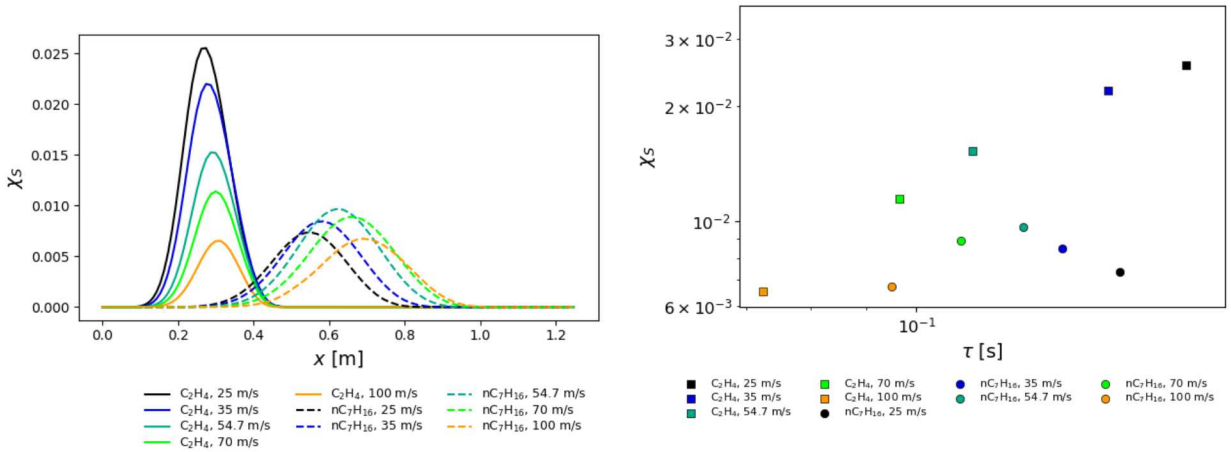

(a) Axial evolution of soot fraction.

(b) Maximum soot fraction as a function of global residence time.

Figure 6: Effect of jet exit velocity on soot fraction evolution and peak values.

The heptane-based simulations have larger flames with increased buoyancy, contributing to fuel-air mixing downstream as noted in Fig. 3. This reduces the change in τ associated with the same change in d/u. The larger volume also increases the radiant fraction relative to the residence time ($\chi_R \propto W_f^2 L_f \alpha T_f^4 \tau$). As the residence time increases, the heptane-based simulations have enough buoyancy and radiation to reduce soot formation. This is a function of the activation energy associated with soot formation with Arrhenius behavior such as $\exp(-11{,}000/T)$; reduced flame temperatures due to radiative cooling are reflected in reduced soot production rates. In the ethene-based simulations the flames are smaller, so there is not enough buoyancy or radiation to limit the soot formation, resulting in the soot formation increasing with increasing residence time. Thus, the ethene simulations directly follow the residence time expectation while the

heptane simulations also demonstrate an interaction with the increased radiant losses.

3.3 Radiation heat losses

As noted in the previous paragraph, radiation and soot formation are closely linked in jet flames. Soot is a major contributor to the jet flame radiation, the other being gas phase radiation. Increased soot formation leads to increased radiation source terms, both for emission and absorption. However, as the radiation losses increase, the flame temperature decreases so less soot can form. To quantify radiation heat losses, we will evaluate the radiant fraction, χ_R, the fraction of the heat of combustion that is lost by the flame through radiation. In the simulations, this is best measured through the change in the flux of enthalpy, h'', minus the adiabatic enthalpy flux expected without radiation heat losses, h''_{ad}. The latter is a linear function of the mixture fraction and can be evaluated using the mixture fraction flux. The flux of enthalpy deficit will be referred to as γ'' and is given by the difference of these two fluxes,

$$\gamma'' = h'' - h''_{ad} = \int_0^\infty \rho u \left[h - h_{ad}(Z)\right] r dr. \tag{10}$$

The radiant fraction is then given by

$$\chi_R = \frac{\gamma''}{Z'' h_C}, \tag{11}$$

where h_C is the heat of combustion. The enthalpy deficit continually increases up to the flame tip with radiant emissions, while the denominator is a conserved quantity equal to the fuel mass flux; thus, the radiant fraction increases along the flame axis. Fig. 7a shows the evolution of the radiant fraction for both fuels and a range of jet velocities. The maximum values from these profiles represent the total radiant fraction, plotted as a function of residence time in Fig. 7b; this value corresponds to the measured radiant fraction in experiments. For both series of flames χ_R increases with τ, and the slope is greater for heptane than ethene.

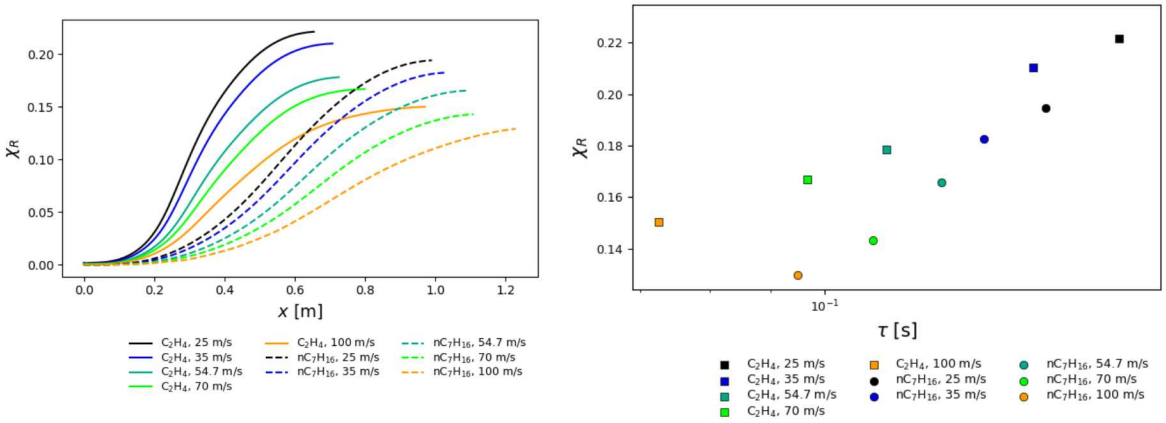

(a) Effect of velocity on radiant fraction.

(b) Radiant fraction versus residence time.

Figure 7: Radiant fraction depends monotonically on residence time and velocity for both fuels considered.

An appropriate radiation time scale is formed from the radiation emission term, the first on the right-hand side of Eq.2, and the heat of combustion. This can be combined with the global residence time, τ, to provide a dimensionless estimate of the radiation losses,

$$R_\tau = \frac{4\sigma\overline{\alpha T^4}\tau}{h_C} \tag{12}$$

that should be similar to the radiant fraction. While it is challenging to estimate a characteristic value for $\overline{\alpha T^4}$, R_τ directly suggests this positive relationship between χ_R and τ shown in Fig. 7b through the linear relationship between R_τ and τ. For these flames that are not optically thick, as the residence time increases the radiant fraction increases more rapidly for heptane. This is attributed here to heptane's greater gas-phase absorption coefficient (noted in the discussion following Eq. 2) and to the greater volume over which the radiation emissions act. This is combined with the smaller overall change in τ attributed to buoyant acceleration.

The magnitudes of the radiant fraction can be compared to measurements available in the literature. We draw on two primary datasets, one with fuels having molar masses similar to ethene [2] and one addressing higher molar mass jet fuels and related surrogate mixtures [3]. Predicted radiant fractions from Fig. 7b are overlaid with these measurements in Fig. 8. The current predictions are within the experimental measurements; they lie in a transition between the shallower dependence of the radiant fraction on the residence time evident in the low molar mass fuels for short residence times [2] and the stronger increase in the radiant fraction observed for longer residence times and the higher molar mass fuels [2, 3]. For the former, especially the methane and CO/H_2 flames, it is expected that radiation is dominated by gas emission and absorption; even with the present ethene and heptane flames the majority of the emissions are from gaseous species. For longer residence times the soot fractions are expected to increase, and for much longer residence times measured in [3] there was a reduced radiant fraction. This might be due to a stronger buoyant mixing effect, or to a stronger radiation reduction in sooting rates as observed for heptane in Fig. 6b, but the current simulations were not conducted at such low Reynolds numbers and Froude numbers. We also note that the lower molar mass fuels including ethene also show an increase in the slope of the radiant fraction versus residence time for residence times above 0.1 s; the current predictions do not show such a strong increase directly, but larger soot production rates do lead to this result as indicated below.

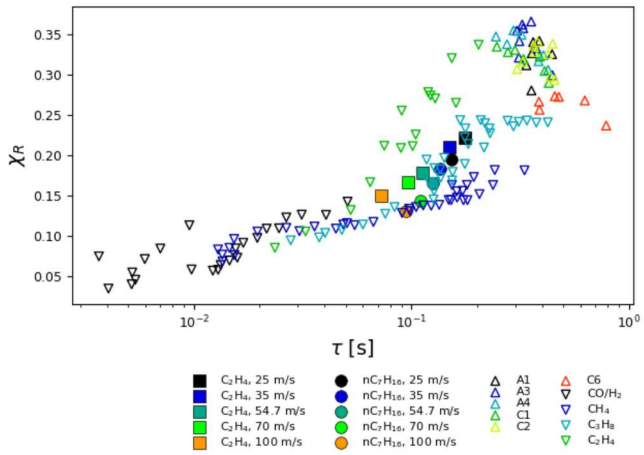

Figure 8: Predicted radiant fractions are compared with measurements available in the literature [2, 3].

3.4 Varying sooting propensity

When considering different fuels, we can adjust the factor r_{sp} to reflect changes in the sooting propensity. Limiting the current results to ethene where the residence time effect is the dominant factor controlling the behavior, we consider the effect of moving r_{sp} from unity to factors of two and four. Only the maximum soot fractions along the flame axes are considered, but the results are determined for the range of exit velocities to give different residence times as well. Results are shown as a function of residence time for

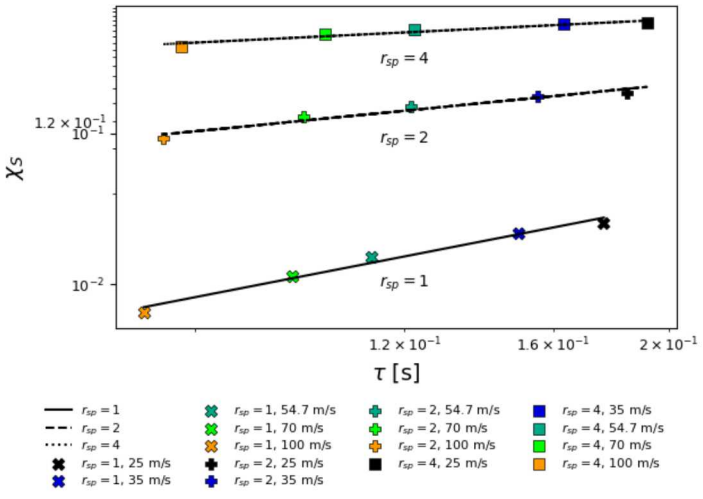

Figure 9: Soot fraction versus residence time for C_2H_4 based fuels for varying sooting propensity.

the different values of r_{sp} in Fig. 9. The residence time of the jet flame limits how much soot can form, and the maximum soot fraction is a monotonically increasing function of the residence time.[1]

However, as the sooting propensity increases, the dependence on the residence time is reduced. This is reflected by taking a power law fit relating the residence time and the maximum soot fraction; results show the exponents on the power law fit are reduced from $\chi_S \propto \tau^{1.54}$ for $r_{sp} = 1$ to $\chi_S \propto \tau^{0.78}$ for $r_{sp} = 2$ to $\chi_S \propto \tau^{0.38}$ for $r_{sp} = 4$. The reduction in the slope is attributed to increased soot radiation with higher soot loading reducing the soot production rates, but unlike heptane, for the smaller ethene flames a positive relation between the soot fraction and the residence time remains. At the same time the total quantity of soot increases dramatically, with the model predicting as much as half of the fuel mass flux converted to soot. This shows a limitation of the model for highly sooting fuels because the current mixture fraction source term allows all of the fuel carbon to be converted to soot. The current model puts a kinetic limit on soot formation and oxidation but does not directly relate that to the kinetics of fuel to CO and H_2 conversion that place upper bounds on the fraction of fuel-derived soot precursors available for soot formation. We note that this results in overpredicted soot levels in our simulations of pool fire (not shown).

The varying sooting propensity also affects the radiant fraction predictions, as expected. As the sooting propensity increases, the radiation heat losses and the resulting maximum radiant fractions increase. These radiant losses provide a feedback mechanism that reduces the soot production for longer residence times, resulting in the reduced power law dependence discussed above. Fig. 10 shows the dependence of the radiant fraction on residence time for varying sooting propensity.

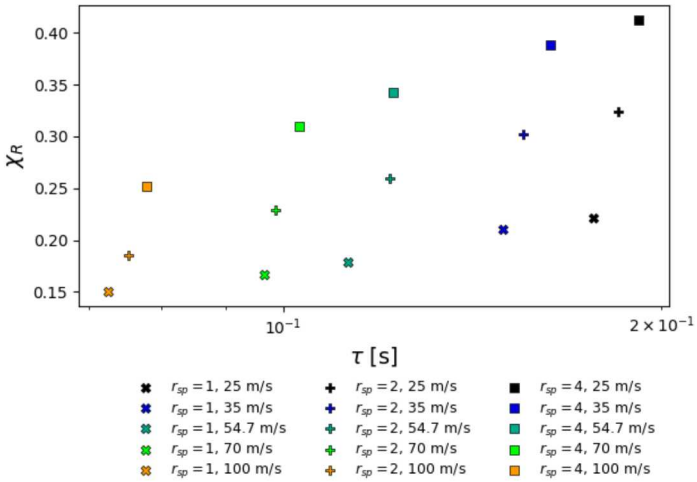

Figure 10: Effect of sooting propensity on radiant fraction.

This limit that soot formation and radiation impose on each other can also be seen in the relationship between radiant fraction and soot fraction shown in Fig. 11. Increasing the soot flux leads to higher radiant fractions, but at higher soot and radiation levels, further soot formation is limited, indicated by the slopes of each r_{sp} series. It is noteworthy that the increase in radiant fraction is small relative to the increase in the soot fraction. Radiant fractions are self limiting because heat losses directly inhibit radiant emissions, while the reduction in soot formation associated with increased radiation, at least for the current model, is not as strong. Soot formation kinetics are not inhibited directly by large soot mass fractions, but the depletion of fuel-derived precursors ultimately places an upper bound on soot formation. The current model form was identified above as not placing a strong enough bound based on fuel-derived precursor depletion.

4. Conclusions

This work examines the predicted trends of relatively simple models for soot formation coupled with radiant heat transfer over a range of residence times and considering a pair of fuel densities that provide some difference in the flame volume for a given residence time. To approximate the role of fuels with different sooting propensities, the soot nucleation and surface growth terms were increased by a factor in some cases;

[1] This is not true for heptane cases as indicated above; with heptane for increased r_{sp} the soot fraction increases and then decreases with increasing residence time, exhibiting similar non-monotonic behavior as shown in Fig. 6b.

this led to a very significant increase in the soot fraction and a more modest increase in the radiant fraction. In general, both soot and radiation tend to increase when global residence times increase as both act independently. However, increased radiation losses can reduce soot formation because soot formation is inhibited if flame temperatures drop low enough. For situations where the relative change in the radiant losses compared to the relative change in the residence time is large enough, the soot fraction does not increase with residence time while the radiant fraction will continue to increase, at least up to a limit where heat losses are already large. For a fixed d/u, larger flames tend to be more buoyant and this leads to a reduced change in residence time; such behavior was observed with higher-density heptane relative to ethene for the current conditions.

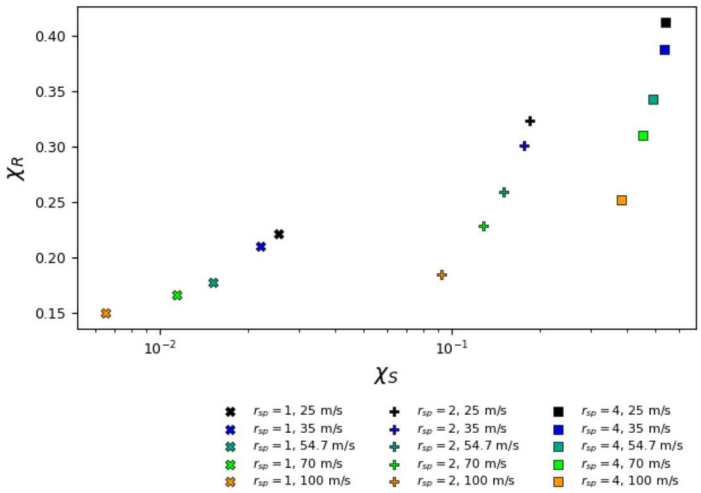

Figure 11: Radiant fraction and soot fraction for various soot factors and velocities.

5. Acknowledgements

The authors gratefully acknowledge funding from the Department of Energy National Nuclear Security Administration Office of Advanced Simulation and Computing. Sandia National Laboratories is a multimission laboratory managed and operated by National Technology and Engineering Solutions of Sandia, LLC., a wholly owned subsidiary of Honeywell International, Inc., for the U.S. Department of Energy's National Nuclear Security Administration under contract DE-NA0003525. This paper describes objective technical results and analysis. Any subjective views or opinions that might be expressed in the paper do not necessarily represent the views of the U.S. Department of Energy or the United States Government.

References

[1] S. M. Mahmoud, G. J. Nathan, Z. T. Alwahabi, Z. W. Sun, P. R. Medwell, and B. B. Dally, The effect of exit strain rate on soot volume fraction in turbulent non-premixed jet flames, Proc. Combust. Instit. 36 (2017) 889–897. DOI: {10.1016/j.proci.2016.08.055}.

[2] S. R. Turns and F. H. Myhr, Oxides of Nitrogen Emissions from Turbulent Jet Flames: Part I, 87 (1991) 319–335.

[3] E. D. Zeuthen and D. L. Blunck, Radiation Emissions from Turbulent Diffusion Flames Burning Vaporized Jet and Jet-like Fuels, Energy Fuels 31 (2017) 1415014160.

[4] N. Peters, Laminar Diffusion Flamelet Models in Nonpremixed Turbulent Combustion, 10 (1984) 319–339.

[5] N. Peters, Turbulent Combustion, Cambridge University Press, Cambridge, United Kingdom, 2000.

[6] M. Fairweather, W. P. Jones, and R. P. Lindstedt, Predictions of radiative transfer from a turbulent reacting jet in a cross-wind, 89 (1992).

[7] J. J. Young and J. B. Moss, Modelling sooting turbulent jet flames using an extended flamlet technique, 105 (1995) 33–53.

[8] S. J. Brookes and J. B. Moss, Predictions of soot and thermal radiation properties in confined turbulent jet diffusion flames, 116 (1999) 486–503.

[9] Z. Wen, S. Yun, M. J. Thompson, and M. F. Lightstone, Modeling soot formation in turbulent kerosene/air jet diffusion flames, Combust. Flame 135 (2003) 323–340.

[10] G. H. Markstein, Relationship Between Smoke Point and Radiant Emissions from Buoyant and Laminar Diffusion Flames, in: The Twentieth Symposium (International) on Combustion, The Combustion Institute, Pittsburgh, 1984, pp. 1055–1061.

[11] C. W. Lautenberger, J. L. de Ris, N. A. Dempsey, J. R. Barnett, and H. R. Baum, Fire Safety Journal 40 (2005) 141–176.

[12] P. Chatterjee, J. L. de Ris, Y. Wang, and S. B. Dorofeev, Proc. Combust. Inst. 33 (2011) 2665–2671.

[13] SIERRA Low Mach Module: Fuego Theory Manual – Version 4.50, SAND2018-12012, tech. rep. Report No., Sandia National Laboratories, 2018.

[14] W. P. Jones and B. E. Launder, Prediction of Laminarization with a 2-Equation Model of Turbulence, Int. J. Heat Mass Transfer 15 (1972) 301.

[15] J. S. T'ien, Diffusion flame extinction at small stretch rates: the mechanism of radiative heat loss, 65 (1986) 31–34.

[16] W. L. Grosshandler, RADCAL: A Narrow-Band Model for Radiation Calculations in a Combustion Environment, tech. rep. Report No., NIST technical note 1402, 1993.

[17] R. S. Barlow, N. S. A. Smith, J.-Y. Chen, and R. W. Bilger, Isolation of the Effects of Radiation and Turbulence-Chemistry Submodels, 117 (1999) 4–31.

[18] I. M. Aksit and J. B. Moss, A hybrid scalar model for sooting turbulent flames, 145 (2006) 231–244. DOI: 10.1016/j.combustflame.2005.10.010.

[19] I. M. Aksit and J. B. Moss, Modeling soot formation in a laminar diffusion flame burning a surrogate kerosene fuel, 31 (2007) 3139–3146.

[20] Yunardi, R. Woolley, and M. Fairweather, Conditional moment closure prediction of soot formation in turbulent, nonpremixed ethylene flames, 152 (2008) 360–376.

[21] J. Zhang, C. R. Shaddix, and R. W. Schefer, Design of "model-friendly" turbulent non-premixed jet burners for C_{2+} *hydrocarbon fuels*, Rev. Sci. Instr. 82 (2011) 074101.

[22] C. R. Shaddix, *ISF-4 target flame 2: Sandia flame*, https://www.adelaide.edu.au/cet/isfworkshop/data-sets/turbulent-flamesisf-4-target-flame-2-sandia-flame, accessed Aug. 30, 2019.

[23] S. M. Mahmoud, G. J. Nathan, Z. T. Alwahabi, Z. W. Sun, P. R. Medwell, and B. B. Dally, The effect of exit strain rate on soot volume fractions in turbulent non-premixed jet flames, Proc. Combust. Instit. 36 (2017) 889–897.